Determination of a CHAMP gravity model based on the Newtonian equation of motion

Lóránt Földváry / *Zsolt* Bokor

Abstract

As the CHAMP has been launched as the first of the gravity satellites of the 2000s, its processing has been a real challenge for the geodetic community. Several methods have been developed for gravity field modelling based on different theoretical backgrounds. In this study the feasibility of the direct use of the Newtonian equation of motion has been studied. Then numerical results for 2 years of CHAMP observations are presented. Though the method failed to provide the best CHAMP-only gravity field model, it has been found to be generally feasible, and worth for using of other gravity satellite data.

Keywords

Newtonian equation of motion · gravity satellite · CHAMP · gravity field modelling

Lóránt Földváry

Department of Geodesy and Surveying, MTA-BME Research Group on Physical Geodesy and Geodynamics, BME, H-1111 Műegyetem Rakpart 3, Budapest, Hungary
e-mail: fl@sci.fgt.bme.hu

Zsolt Bokor

University of West Hungary, Bajcsy-Zsilinszky u. 4., H-9400 Sopron,, Hungary
e-mail: info@tavmero.hu

1 Introduction

Generally, the first decade of the new century has provided some of the most exciting satellite missions of the space geodesy. The CHAMP satellite aimed to determine the magnetic field of the Earth, but also allows the determination of the gravity field. The CHAMP is followed by the GRACE, which is a definite satellite gravimetric mission, which provides both a very accurate static and a set of monthly varying gravity fields. The finally launched mission was the GOCE gradiometric mission, which concentrates on the static field with very detailed resolution. An appropriate combination of the gain of these gravity missions can provide a very accurate global gravity model, enabling a range of scientific applications on global sense [19]; [5]. Furthermore, due to their unprecedented spatial resolution, i.e. some cm accuracy of geoid on some 100 km scale, these measurements can effectively support refinement of a regional geoid model [9]; [20]; [24], which can be extensively used as the reference height level for different scientific and engineering applications (e.g. [22]; [2]).

As the CHAMP has been launched first, its processing has been a challenge for the geodetic community. Several methods have been developed for different theoretical backgrounds. The energy integral approach has already been employed in the Hungarian research community as well [8]; [12] and [13], while the use of the Newtonian equation of motion is a novelty for us. Though different groups have derived their method making use of the equation of motion, no detailed description of the method or essentially different methods under the same name has been found (e.g. [1]; [17]). Elaborated description of the method as derived by us and numerical results for CHAMP observations are introduced and discussed in the present study.

The CHAMP satellite has been launched on 15. July of 2000. The CHAMP satellite (Fig. 1) has a special characteristic due to the long rod in its front, the so-called "boom". The boom has been attached for bearing one of the main on-board instruments, the magnetometer, which means an unlike profile for gravimetric applications. Some technical parameters are listed in the table next to Fig. 1. The choice of the inclination reflects the no need of overemphasis of the polar region, while the al-

titude (from 460 km gradually shifted to 250-300 km) provides the very good resolution.
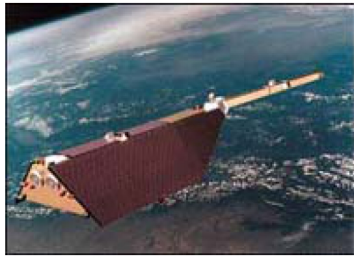
Launch:	15.07.2000.
Altitude:	460 km
Inclination:	87.3°
Mass:	522 kg
Length:	8 m (with the Boom)
Nominal duration:	7 yr
Control centres:	DLR / GSOC
Control station:	Weilheim, Neustrelitz

Fig. 1. The CHAMP satellite and some technical parameters

We have used two years of CHAMP measurements in the period of 11.03.2002 and 29.02.2004. The data base contained orbit determined with precise GPS in 30 s resolution and measurements of the on-board accelerometer.

2 Equation of motion of the satellite

In a conservative force field (or inertial field) all the forces, $\mathbf{f}$ have a regular potential field, V, so $\mathbf{f} = \nabla V$ holds. According to this, the acceleration of the satellite, $\ddot{\mathbf{x}}$ can be assumed to be generated by the gradient of the potential field.

$$\ddot{\mathbf{x}} = \nabla V \tag{1}$$

Since for most application in geosciences the use of Earth-fixed coordinate system is unavoidable, in the following parts the equation of motion is derived in a rotating reference frame.

2.1 Equation of motion of the satellite in a rotating frame

The Earth-fixed reference frame is a rotating system, so Eq. (1) does not hold. From now on the rotating system is noted with X, Y, Z coordinates, while for the inertial system x, y, z axes are used. Accelerations in the rotating system and in the inertial systems can be related to each other [18]:

$$\ddot{\mathbf{r}}_{XYZ} = \mathbf{R}\ddot{\mathbf{r}}_{xyz} - 2\left(\boldsymbol{\omega} \times \dot{\mathbf{r}}_{XYZ}\right) - \left(\dot{\boldsymbol{\omega}} \times \mathbf{r}_{XYZ}\right) - \boldsymbol{\omega} \times \left(\boldsymbol{\omega} \times \mathbf{r}_{XYZ}\right), \tag{2}$$

where $\boldsymbol{\omega}$ is the angular velocity of the rotating Earth, "dot" refers to differentiation with respect to time, and $\mathbf{R}$ is the rotational matrix, thus $\mathbf{r}_{XYZ} = \mathbf{R}\mathbf{r}_{xyz}$. All components of Eq. (2) can be interpreted from physical aspect. According to Eq. (2), acceleration observed in a rotational, $\ddot{\mathbf{r}}_{XYZ}$ and in an inertial coordinate system, $\ddot{\mathbf{r}}_{xyz}$ are different in the following terms: $-2\left(\boldsymbol{\omega} \times \dot{\mathbf{r}}_{XYZ}\right)$, the Coriolis acceleration, $-\left(\dot{\boldsymbol{\omega}} \times \mathbf{r}_{XYZ}\right)$, the Euler acceleration and $-\boldsymbol{\omega} \times \left(\boldsymbol{\omega} \times \mathbf{r}_{XYZ}\right)$, the centrifugal acceleration.

Applying Eq. 2) for the equation of the motion of a satellite, Eq. (1) becomes:

$$\nabla V = \mathbf{R}\ddot{\mathbf{x}} - 2\left(\boldsymbol{\omega} \times \dot{\mathbf{X}}\right) - \left(\dot{\boldsymbol{\omega}} \times \mathbf{X}\right) - \boldsymbol{\omega} \times \left(\boldsymbol{\omega} \times \mathbf{X}\right). \tag{3}$$

2.2 Equation of motion of the satellite in a non-conservative force field

In case of a non-conservative force field, acceleration of a point mass is generated by the sum of all the accelerations acting on it, so

$$\ddot{\mathbf{x}} = \nabla V + \sum \mathbf{f}_{nc}, \tag{4}$$

or in the case of a rotating system

$$\mathbf{R}\ddot{\mathbf{x}} - 2\left(\boldsymbol{\omega} \times \dot{\mathbf{X}}\right) - \left(\dot{\boldsymbol{\omega}} \times \mathbf{X}\right) - \boldsymbol{\omega} \times \left(\boldsymbol{\omega} \times \mathbf{X}\right) = \nabla V + \sum \mathbf{f}_{nc}, \tag{5}$$

where $\sum \mathbf{f}_{nc}$ stands for the sum of the non-conservative accelerations, the subscript nc refers to "non-conservative". On board of the CHAMP there is a capacitive accelerometer used to detect the non-conservative accelerations, therefore the sum of these effects can be treated without considering the different and independent sources separately.

2.3 Equation of motion of the satellite in force field of certain celestial bodies

In Eq. (5) all conservative accelerations are summed in the term ∇V. Among them the largest is by far the gravitational acceleration of the Earth, moreover for geodetic use this is the target quantity to be determined. Therefore it is worth to decompose ∇V into its sources. First of all the satellite is affected by the force field of more celestial bodies, these are the so-called tides. Secondly, these celestial bodies generate mass redistributions of the physical body of the Earth, these are the indirect tides, such as ocean tides, solid Earth tides. Finally the celestial bodies by their effect on the mass distribution indirectly relocate the rotational axis of the Earth – this type of indirect tide is the pole motion. So Eq. (5) by noting the separated effects becomes:

$$\begin{aligned} \mathbf{R}\ddot{\mathbf{x}} - 2\left(\boldsymbol{\omega} \times \dot{\mathbf{X}}\right) - \left(\dot{\boldsymbol{\omega}} \times \mathbf{X}\right) - \boldsymbol{\omega} \times \left(\boldsymbol{\omega} \times \mathbf{X}\right) \\ = \nabla V_{Earth} + \nabla V_{ls} + \nabla V_{ind} + \sum \mathbf{f}_{nc}, \end{aligned} \tag{6}$$

where ∇V_{Earth} is the gravitational acceleration of the Earth, ∇V_{ls} is the direct tide effect of the other celestial bodies (*ls* refers to *lunisolar* as the main contribution is provided by the Sun and the Moon), ∇V_{ind} refers to the indirect tides, including the ocean tide, the solid Earth tide and the polar motion.

3 Equation of motion of the satellite as observation equation for determining the gravity field by spherical harmonic analysis

Rearranging Eq. (6) for the gravitational acceleration becomes:

$$\begin{aligned} \nabla V_{Earth} = \mathbf{R}\ddot{\mathbf{x}} - 2\left(\boldsymbol{\omega} \times \dot{\mathbf{X}}\right) - \left(\dot{\boldsymbol{\omega}} \times \mathbf{X}\right) - \boldsymbol{\omega} \times \left(\boldsymbol{\omega} \times \mathbf{X}\right) \\ - \nabla V_{ls} - \nabla V_{ind} - \sum \mathbf{f}_{nc}. \end{aligned} \tag{7}$$

All the terms in the right hand side can be considered by measured or modelled quantities. The acceleration of the satellite can be derived from the orbit of the satellite by numerical differentiation. The Earth-related parameters of the centrifugal, Euler and Coriolis accelerations are provided by the IERS (International Earth Rotation and Reference Systems Service) [11]. Values of ∇V_{ls} and ∇V_{ind} can be derived from tide models. The

non-conservative accelerations, $\sum \mathbf{f}_{nc}$ are measured by the on-board accelerometer. These measured and modelled effects can be summed in an observation vector:

$$\mathbf{I} = \mathbf{R}\ddot{\mathbf{x}} - 2\left(\boldsymbol{\omega} \times \dot{\mathbf{X}}\right) - \left(\dot{\boldsymbol{\omega}} \times \mathbf{X}\right) - \boldsymbol{\omega} \times \left(\boldsymbol{\omega} \times \mathbf{X}\right)$$
$$- \nabla V_{ls} - \nabla V_{ind} - \sum \mathbf{f}_{nc}. \tag{8}$$

So Eq. (7) – with leaving the trivial notation that the potential refers to that of the Earth – simplifies to:

$$\nabla V = \mathbf{I}, \tag{9}$$

where V can be defined in the usual spherical harmonic representation (e.g. [19]). The adjustment is done for a set of unknowns, $\bar{C}_{lm}$ and $\bar{S}_{lm}$ normalized spherical harmonic coefficients. Therefore analytical determination of ∇V, and of the partial derivatives, $\frac{\partial \nabla V}{\partial \langle \bar{C}_{lm}, \bar{S}_{lm} \rangle}$ should be provided. The gradient of the potential in a rectangular coordinate system is:

$$\nabla V = \begin{bmatrix} \frac{\partial V}{\partial x} \\ \frac{\partial V}{\partial y} \\ \frac{\partial V}{\partial z} \end{bmatrix} = \begin{bmatrix} \frac{\partial V}{\partial r}\frac{dr}{dx} + \frac{\partial V}{\partial \varphi}\frac{d\varphi}{dx} + \frac{\partial V}{\partial \lambda}\frac{d\lambda}{dx} \\ \frac{\partial V}{\partial r}\frac{dr}{dy} + \frac{\partial V}{\partial \varphi}\frac{d\varphi}{dy} + \frac{\partial V}{\partial \lambda}\frac{d\lambda}{dy} \\ \frac{\partial V}{\partial r}\frac{dr}{dz} + \frac{\partial V}{\partial \varphi}\frac{d\varphi}{dz} + \frac{\partial V}{\partial \lambda}\frac{d\lambda}{dz} \end{bmatrix}. \tag{10}$$

The partial derivatives with respect to the polar coordinates are

$$\frac{\partial V}{\partial r} = -\frac{kM}{R^2}\sum_{l=0}^{\infty} l\left(\frac{R}{r}\right)^{l+1}\sum_{m=0}^{l}\begin{pmatrix} \bar{C}_{lm}\cos m\lambda \\ \bar{S}_{lm}\sin m\lambda \end{pmatrix}\bar{P}_{lm}(\varphi)$$

$$\frac{\partial V}{\partial \varphi} = \frac{kM}{R}\sum_{l=0}^{\infty}\left(\frac{R}{r}\right)^{l}\sum_{m=0}^{l}\begin{pmatrix} \bar{C}_{lm}\cos m\lambda \\ \bar{S}_{lm}\sin m\lambda \end{pmatrix}\frac{\partial \bar{P}_{lm}(\varphi)}{\partial \varphi} \tag{11}$$

$$\frac{\partial V}{\partial \lambda} = \frac{kM}{R}\sum_{l=0}^{\infty}\left(\frac{R}{r}\right)^{l}\sum_{m=0}^{l}\begin{pmatrix} -m\bar{C}_{lm}\sin m\lambda \\ m\bar{S}_{lm}\cos m\lambda \end{pmatrix}\bar{P}_{lm}(\varphi)$$

The remaining components of Eq. (10), which describes the transformation between the Cartesian and the polar coordinates is the well-known:
$$\begin{bmatrix} x \\ y \\ z \end{bmatrix} = \begin{bmatrix} r\cos\varphi\cos\lambda \\ r\cos\varphi\sin\lambda \\ r\sin\varphi \end{bmatrix}$$
or
$$\begin{bmatrix} r \\ \varphi \\ \lambda \end{bmatrix} = \begin{bmatrix} \sqrt{x^2+y^2+z^2} \\ \arctan\frac{z}{d} \\ \arctan\frac{y}{x} \end{bmatrix},$$
where $d = \sqrt{x^2+y^2}$. According to this in Eq. (10) the derivatives of the polar coordinates with respect to the Cartesian ones are the followings:

$$\begin{bmatrix} \frac{dr}{dx} \\ \frac{d\varphi}{dx} \\ \frac{d\lambda}{dx} \end{bmatrix} = \begin{bmatrix} \frac{x}{r} \\ \frac{-zx}{r^2d} \\ \frac{-y}{d^2} \end{bmatrix}; \quad \begin{bmatrix} \frac{dr}{dy} \\ \frac{d\varphi}{dy} \\ \frac{d\lambda}{dy} \end{bmatrix} = \begin{bmatrix} \frac{y}{r} \\ \frac{-zy}{r^2d} \\ \frac{x}{d^2} \end{bmatrix};$$
$$\begin{bmatrix} \frac{dr}{dz} \\ \frac{d\varphi}{dz} \\ \frac{d\lambda}{dz} \end{bmatrix} = \begin{bmatrix} \frac{z}{r} \\ \frac{d}{r^2} \\ 0 \end{bmatrix}, \tag{12}$$

or in a different notation [21]:

$$\begin{bmatrix} \frac{dr}{dx} \\ \frac{d\varphi}{dx} \\ \frac{d\lambda}{dx} \end{bmatrix} = \begin{bmatrix} \cos\varphi\cos\lambda \\ -\frac{\sin\varphi\cos\lambda}{r} \\ -\frac{\sin\lambda}{r\cos\varphi} \end{bmatrix}; \quad \begin{bmatrix} \frac{dr}{dy} \\ \frac{d\varphi}{dy} \\ \frac{d\lambda}{dy} \end{bmatrix} = \begin{bmatrix} \cos\varphi\sin\lambda \\ -\frac{\sin\varphi\sin\lambda}{r} \\ \frac{\cos\lambda}{r\cos\varphi} \end{bmatrix};$$
$$\begin{bmatrix} \frac{dr}{dz} \\ \frac{d\varphi}{dz} \\ \frac{d\lambda}{dz} \end{bmatrix} = \begin{bmatrix} \sin\varphi \\ \frac{\cos\varphi}{r} \\ 0 \end{bmatrix}. \tag{13}$$

The partial derivatives required for the design matrix with the use of Eq. (10) and (11) becomes:

$$\frac{\partial \nabla V}{\partial \begin{pmatrix} \bar{C}_{lm} \\ \bar{S}_{lm} \end{pmatrix}} = \begin{bmatrix} \frac{\partial\left(\frac{\partial V}{\partial r}\frac{dr}{dx} + \frac{\partial V}{\partial \varphi}\frac{d\varphi}{dx} + \frac{\partial V}{\partial \lambda}\frac{d\lambda}{dx}\right)}{\partial\begin{pmatrix} \bar{C}_{lm} \\ \bar{S}_{lm} \end{pmatrix}} \\ \frac{\partial\left(\frac{\partial V}{\partial r}\frac{dr}{dy} + \frac{\partial V}{\partial \varphi}\frac{d\varphi}{dy} + \frac{\partial V}{\partial \lambda}\frac{d\lambda}{dy}\right)}{\partial\begin{pmatrix} \bar{C}_{lm} \\ \bar{S}_{lm} \end{pmatrix}} \\ \frac{\partial\left(\frac{\partial V}{\partial r}\frac{dr}{dz} + \frac{\partial V}{\partial \varphi}\frac{d\varphi}{dz} + \frac{\partial V}{\partial \lambda}\frac{d\lambda}{dz}\right)}{\partial\begin{pmatrix} \bar{C}_{lm} \\ \bar{S}_{lm} \end{pmatrix}} \end{bmatrix} =$$

$$= \frac{kM}{R}\sum_{l=0}^{\infty}\sum_{m=0}^{l}\left(\frac{R}{r}\right)^{l}\bar{P}_{lm}(\varphi)$$

$$\cdot \begin{bmatrix} -\frac{l}{r}\begin{pmatrix} \cos m\lambda \\ \sin m\lambda \end{pmatrix}\frac{dr}{dx} + \begin{pmatrix} \cos m\lambda \\ \sin m\lambda \end{pmatrix}\frac{\partial\bar{P}_{lm}(\varphi)}{\partial\varphi}\frac{1}{\bar{P}_{lm}(\varphi)}\frac{d\varphi}{dx} + \begin{pmatrix} -m\sin m\lambda \\ m\cos m\lambda \end{pmatrix}\frac{d\lambda}{dx} \\ -\frac{l}{r}\begin{pmatrix} \cos m\lambda \\ \sin m\lambda \end{pmatrix}\frac{dr}{dy} + \begin{pmatrix} \cos m\lambda \\ \sin m\lambda \end{pmatrix}\frac{\partial\bar{P}_{lm}(\varphi)}{\partial\varphi}\frac{1}{\bar{P}_{lm}(\varphi)}\frac{d\varphi}{dy} + \begin{pmatrix} -m\sin m\lambda \\ m\cos m\lambda \end{pmatrix}\frac{d\lambda}{dy} \\ -\frac{l}{r}\begin{pmatrix} \cos m\lambda \\ \sin m\lambda \end{pmatrix}\frac{dr}{dz} + \begin{pmatrix} \cos m\lambda \\ \sin m\lambda \end{pmatrix}\frac{\partial\bar{P}_{lm}(\varphi)}{\partial\varphi}\frac{1}{\bar{P}_{lm}(\varphi)}\frac{d\varphi}{dz} + \begin{pmatrix} -m\sin m\lambda \\ m\cos m\lambda \end{pmatrix}\frac{d\lambda}{dz} \end{bmatrix}. \tag{14}$$

In the next steps simplifications of Eq. (14) are to be provided. Symmetry of (11) with the spherical harmonic representation of the potential suggests that partial derivatives of the potential should be derived as a function of the potential itself.

$$\frac{\partial V_{lm}}{\partial r} = -\frac{l+1}{r}V_{lm}$$

$$\frac{\partial V_{lm}}{\partial \varphi} = \frac{\partial\bar{P}_{lm}(\varphi)}{\partial\varphi}\frac{1}{\bar{P}_{lm}(\varphi)}V_{lm} \tag{15}$$

$$\frac{\partial V_{lm}}{\partial \lambda} = \begin{pmatrix} -m\tan m\lambda \\ m\cot m\lambda \end{pmatrix}V_{lm}$$

Using (15) and (12) or (13) the partial derivatives become (for use of (12) and (13) the result is (16) and (17), respectively):

$$\frac{\partial \nabla V}{\partial \begin{pmatrix} \bar{C}_{lm} \\ \bar{S}_{lm} \end{pmatrix}} =$$

$$\begin{bmatrix} -\frac{l+1}{r^2}x - \frac{\partial\bar{P}_{lm}(\varphi)}{\partial\varphi}\frac{zx}{r^2d\bar{P}_{lm}(\varphi)} - \begin{pmatrix} -m\tan m\lambda \\ m\cot m\lambda \end{pmatrix}\frac{y}{d^2\cos\varphi} \\ -\frac{l+1}{r^2}y - \frac{\partial\bar{P}_{lm}(\varphi)}{\partial\varphi}\frac{zy}{r^2d\bar{P}_{lm}(\varphi)} + \begin{pmatrix} -m\tan m\lambda \\ m\cot m\lambda \end{pmatrix}\frac{x}{d^2\cos\varphi} \\ -\frac{l+1}{r^2}z + \frac{\partial\bar{P}_{lm}(\varphi)}{\partial\varphi}\frac{d}{r^2\bar{P}_{lm}(\varphi)} \end{bmatrix}\frac{\partial V_{lm}}{\partial\begin{pmatrix} \bar{C}_{lm} \\ \bar{S}_{lm} \end{pmatrix}} \tag{16}$$

$$\frac{\partial \nabla V}{\partial \left(\begin{array}{c} \bar{C}_{lm} \\ \bar{S}_{lm} \end{array} \right)} =$$

$$\left[\begin{array}{c} -\frac{l+1}{r}\cos\varphi\cos\lambda - \frac{\partial \bar{P}_{lm}(\varphi)}{\partial \varphi}\frac{\sin\varphi\cos\lambda}{r\bar{P}_{lm}(\varphi)} - \left(\begin{array}{c} -m\tan m\lambda \\ m\cot m\lambda \end{array} \right) \frac{\sin\lambda}{r\cos\varphi} \\ -\frac{l+1}{r}\cos\varphi\sin\lambda - \frac{\partial \bar{P}_{lm}(\varphi)}{\partial \varphi}\frac{\sin\varphi\sin\lambda}{r\bar{P}_{lm}(\varphi)} + \left(\begin{array}{c} -m\tan m\lambda \\ m\cot m\lambda \end{array} \right) \frac{\cos\lambda}{r\cos\varphi} \\ -\frac{l+1}{r}\sin\varphi + \frac{\partial \bar{P}_{lm}(\varphi)}{\partial \varphi}\frac{\cos\varphi}{r\bar{P}_{lm}(\varphi)} \end{array} \right] \frac{\partial V_{lm}}{\partial \left(\begin{array}{c} \bar{C}_{lm} \\ \bar{S}_{lm} \end{array} \right)}$$

(17)

Inserting the spherical harmonic series of the potential to (16) or (17), furthermore using the simple geometrical equation, $d^2 = x^2 + y^2 = r^2 \cos^2 \varphi$, the design matrix can be built using the formulas below (for use of (16) and (17) the result is (18) and (19), respectively):

$$\frac{\partial \nabla V}{\partial \left(\begin{array}{c} \bar{C}_{lm} \\ \bar{S}_{lm} \end{array} \right)} =$$

$$\left[\begin{array}{c} -(l+1)x - \frac{\partial \bar{P}_{lm}(\varphi)}{\partial \varphi}\frac{zx}{d\bar{P}_{lm}(\varphi)} - \left(\begin{array}{c} -m\tan m\lambda \\ m\cot m\lambda \end{array} \right) \frac{y}{\cos^3\varphi} \\ -(l+1)y - \frac{\partial \bar{P}_{lm}(\varphi)}{\partial \varphi}\frac{zy}{d\bar{P}_{lm}(\varphi)} + \left(\begin{array}{c} -m\tan m\lambda \\ m\cot m\lambda \end{array} \right) \frac{x}{\cos^3\varphi} \\ -(l+1)z + \frac{\partial \bar{P}_{lm}(\varphi)}{\partial \varphi}\frac{d}{\bar{P}_{lm}(\varphi)} \end{array} \right]$$

$$\cdot \frac{kM}{R^3}\left(\frac{R}{r} \right)^{l+3} \left(\begin{array}{c} \cos m\lambda \\ \sin m\lambda \end{array} \right) \bar{P}_{lm}(\varphi)$$

(18)

$$\frac{\partial \nabla V}{\partial \left(\begin{array}{c} \bar{C}_{lm} \\ \bar{S}_{lm} \end{array} \right)} =$$

$$\frac{kM}{R^2}\left[\begin{array}{c} -(l+1)\cos\varphi\cos\lambda - \frac{\partial \bar{P}_{lm}(\varphi)}{\partial \varphi}\frac{\sin\varphi\cos\lambda}{\bar{P}_{lm}(\varphi)} - \left(\begin{array}{c} -m\tan m\lambda \\ m\cot m\lambda \end{array} \right) \frac{\sin\lambda}{\cos\varphi} \\ -(l+1)\cos\varphi\sin\lambda - \frac{\partial \bar{P}_{lm}(\varphi)}{\partial \varphi}\frac{\sin\varphi\sin\lambda}{\bar{P}_{lm}(\varphi)} + \left(\begin{array}{c} -m\tan m\lambda \\ m\cot m\lambda \end{array} \right) \frac{\cos\lambda}{\cos\varphi} \\ -(l+1)\sin\varphi + \frac{\partial \bar{P}_{lm}(\varphi)}{\partial \varphi}\frac{\cos\varphi}{\bar{P}_{lm}(\varphi)} \end{array} \right]$$

$$\cdot \left(\frac{R}{r} \right)^{l+1} \left(\begin{array}{c} \cos m\lambda \\ \sin m\lambda \end{array} \right) \bar{P}_{lm}(\varphi)$$

(19)

4 Results

4.1 Observation vector

The largest contribution of the observation vector is provided by the kinematic acceleration of the satellite, $\ddot{\mathbf{x}}$, which has been determined as in [6]. An order of magnitude smaller signal provided by the centrifugal, Euler and Coriolis accelerations. In case of the Euler acceleration the angular acceleration, $\dot{\boldsymbol{\omega}}$, has been derived from the IERS angular velocity data by simple linear interpolation, which rough method has been found sufficiently accurate with respect to the tiny magnitude of the signal.

The contribution of the direct tidal effects is even smaller, i.e. in the order of 10^{-6} m/s^2. Practically effects of the Sun, Moon, Jupiter, Mars, Venus and Saturn have been taken into account. In all cases 12 hour ephemeris data were available, and to the actual epoch the data have been interpolated by linear interpolation.

The indirect tides, ∇V_{ind} are an order of magnitude below the direct tides. The solid Eatrh tide and polar motion was computed

as suggested by the IERS [11]. The ocean tide based on the Schwiderski combined with TOPEX/Poseidon tide model.

The non-conservative accelerations, $\sum \mathbf{f}_{nc}$ are similar to the order of the direct tides. Observations of the accelerometer are presented in 1 second resolution, which we have reduced to 30 seconds with a Butterworth-filter.
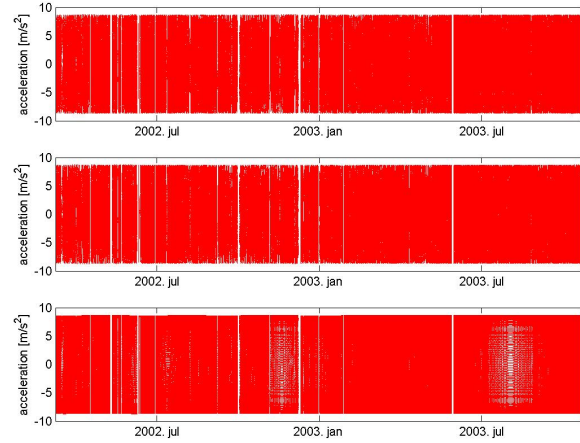
Fig. 2. CHAMP-based gravitational acceleration along X, Y and Z axes (up to down)

In Fig. 2 the observation vector is visualized as described by Eq. (8). This value is the basis of the gravity analysis, thus it manifests the gravitation of the Earth as detected by the CHAMP. This is compared to a synthesised signal from a known Earth gravitation model on Fig. 3, where differences of ∇V from CHAMP and from a model are displayed. The used gravity model is the EGM96 [10]. The information on Fig. 3 is two kinds: first, it displays the signal, which is the novel information on the gravity field to the EGM96 model. Second it also shows all the CHAMP measurement, processing and modelling errors. This information of the second kind is overemphasized: the visible "large" variation in the range of 0.01 m/s^2, is mainly contributed by outliers contributing only to the very short wavelength gravity information, which in practice makes no harm on the gravity analysis.

4.2 Pre-processing

The two years of CHAMP observations have been filtered in order to omit data gaps and outliers. Data gaps both in the orbit and in the star catalogue have been detected. Outlier of the orbit has been defined as deviation to a physically meaningful orbit, i.e. the kinematic orbit has been filtered by comparing to a reduced-dynamic orbit, which is known to be accurate to some centimetres. The maximal deviation has been set to 0.5 m. All together 26% of the data has been filtered. The remaining epochs contain valid data for applying Eqs. (8) and (19) on them to build the observation vector and the design matrix, respectively.

According to a priori information on the content of the
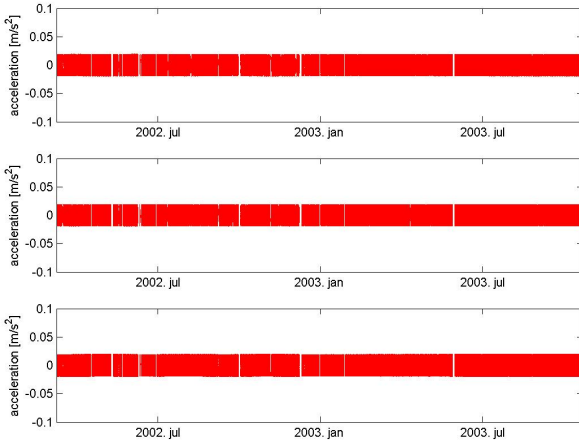
Fig. 3. Gravitational acceleration residuals (CHAMP minus EGM96) along X, Y and Z axes (up to down)

CHAMP measurements [7] the maximal degree and order of the spherical harmonic analysis has been set to 60, which means 3721 unknowns.

4.3 Normal matrix
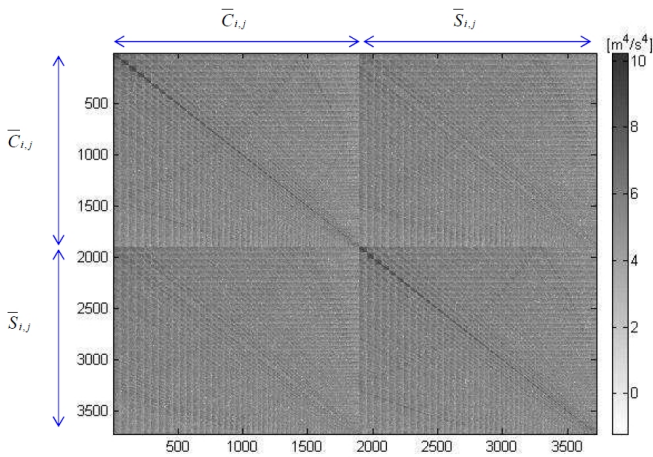
Fig. 4. The normal matrix

The normal matrix has been derived from the design matrix based on Eq. (19) by assuming unit weights, so $\mathbf{N} = \mathbf{A}^T\mathbf{A}$. Since the size of the design matrix is too large to be treated by a regular PC, we have determined directly the normal matrix instead for more details see [3]. This has been done by the dyadic decomposition of the design matrix [4]. The determined normal matrix is shown on Fig. 4 in logarithmic scale. The sequencing scheme of the normal matrix by degree and order is explained on Table 1.

Tab. 1. Sequencing scheme of the coefficients on Figs. 4 and 5.

The block diagonal structure of the normal matrix is to the expectations, manifesting the large correlation of the coefficients with the same order. The other characteristic feature is the curved lines showing the resonances; those coefficients cannot be determined from the CHAMP orbit. At these places the orbit geometry purely mathematically provides incredible large coefficients [23].

The observation vector computed by $\mathbf{n} = \mathbf{A}^T\mathbf{l}$ is shown on Fig. 5 in the same sequence (cf. Table 1). The figure shows that the energy of the gravitational field is concentrated to the long wavelength.
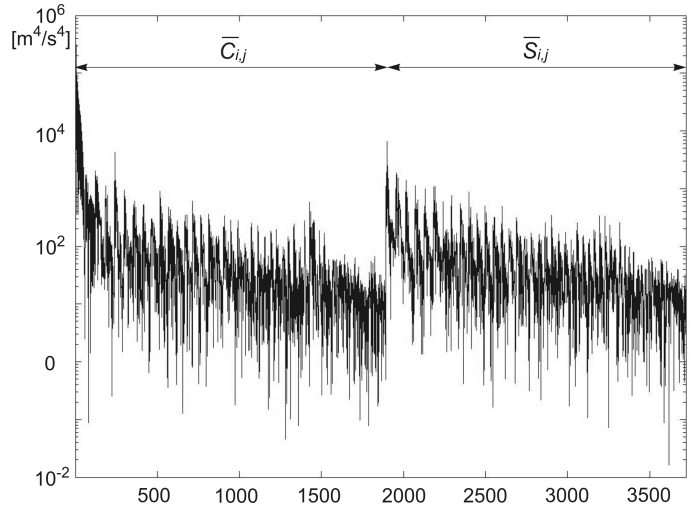
Fig. 5. The observation vector

4.4 CHAMP gravity model

Using the normal matrix (Fig. 4) and the observation vector (Fig. 5) the unknowns determined by $\mathbf{x} = \mathbf{N}^{-1}\mathbf{n}$ are displayed on Fig. 6 in a logarithmic scale in the usual sequencing scheme, i.e.:

$$
\begin{bmatrix}
\bar{C}_{0,0} & \bar{S}_{1,1} & \bar{S}_{2,1} & \dots & \bar{S}_{i,1} & \dots & \bar{S}_{59,1} & \bar{S}_{60,1} \\
\bar{C}_{1,0} & \bar{C}_{1,1} & \bar{S}_{2,2} & \dots & \bar{S}_{i,2} & \dots & \bar{S}_{59,2} & \bar{S}_{60,2} \\
\bar{C}_{2,0} & \bar{C}_{2,1} & \bar{C}_{2,2} & \dots & \bar{S}_{i,3} & \dots & \bar{S}_{59,3} & \bar{S}_{60,3} \\
\dots & \dots & \dots & \dots & \dots & \dots & \dots & \dots \\
\bar{C}_{i,0} & \bar{C}_{i,1} & \bar{C}_{i,2} & \dots & \bar{C}_{i,i} & \dots & \bar{S}_{59,i+1} & \bar{S}_{60,i+1} \\
\dots & \dots & \dots & \dots & \dots & \dots & \dots & \dots \\
\bar{C}_{59,0} & \bar{C}_{59,1} & \bar{C}_{59,2} & \dots & \bar{C}_{59,i} & \dots & \bar{C}_{59,59} & \bar{S}_{60,60} \\
\bar{C}_{60,0} & \bar{C}_{60,1} & \bar{C}_{60,2} & \dots & \bar{C}_{60,i} & \dots & \bar{C}_{60,59} & \bar{C}_{60,60}
\end{bmatrix}.
$$

The geoid based on the newly derived coefficients is shown on Fig. 7.

5 Discussions and conclusions

The validation of the newly derived geoid has been done by comparison with known gravity models. The comparison was done on geoids. The used models are EGM96 [10], EIGEN-1S [14], EIGEN-2 [15] and EIGEN-GRACE01S [16]. In Table 2 the standard deviations are summarized.
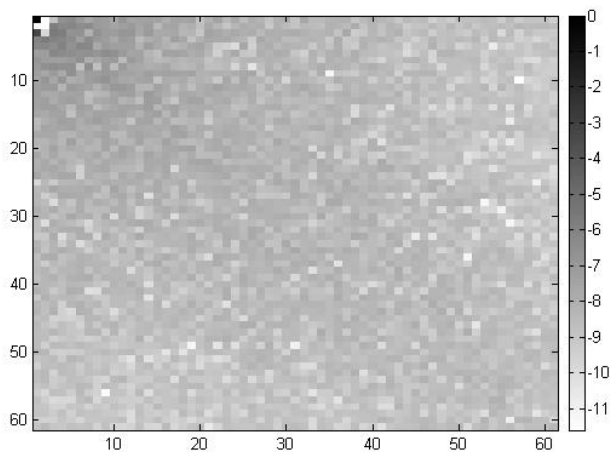
Fig. 6. The CHAMP coefficients
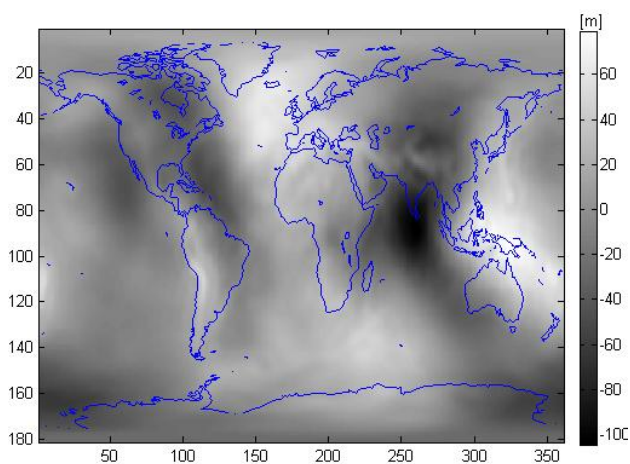
Fig. 7. The CHAMP geoid

Tab. 2. The standard deviation of the different geoids to our model

Model	EGM96	EIGEN-1S	EIGEN-2	EIGEN-GRACE01S
std. dev [cm]	63.4	29.3	39.7	52.9

According to the statistics, there is a clear correlation with the other CHAMP models. Surprisingly this CHAMP solution shows more similarity to two other CHAMP-based models (EIGEN-1S and EIGEN-2) than the two to each other, which has been found to be +/- 53.9 cm (not included in Table 2). Assuming that the state-of-the-art GRACE model (EIGEN-GRACE01S) is the most accurate among these models, the statistics with using this model as a reference has also been determined (Table 3).

Tab. 3. The standard deviation of the different geoids to EIGEN-GRACE01S

Model	EGM96	EIGEN-1S	EIGEN-2	THIS MODEL
std. dev [cm]	38.2	61.9	41.1	52.9

According to this table we can conclude that this solution in accuracy lies between the first two official CHAMP releases. This is a fairly good result, even though finally we did not yield the best possible result from certain satellite data. The method is worth to apply to the orbit of other gravity satellites by redefining it for the specialization of them. For the GRACE measurements between the two satellites can be involved by changing Eq. (7) from the gradient of the potential to that of potential difference at the location of the two satellites. In the case of the GOCE the method can directly be applied for the GOCE SST part coupled with a GOCE SGG solution. In these other cases the method can be more successfully applied just due to the differences in the orbit geometry.

References

1 **Austen G, Grafarend E W, Reubelt T**, *Analysis of the Earth's Gravitational Field from Semi-continuous Ephemeris of a Low Earth Orbiting GPS-tracked Satellite of Type CHAMP, GRACE or GOCE*, Vistas for Geodesy in the New Millennium (Ádám J, Schwarz K P, eds.), IAG Symposia, vol. 125, Springer-Verlag, Berlin-Heidelberg, 2002, pp. 309–315.

2 **Berényi A, Lovas T, Barsi Á, Dunai T**, *Potential of terrestrial laserscanning in load test measurements of bridges*, Per. Pol. Civil Eng. **53** (2009), no. 1, 25–33, DOI 10.3311/pp.ci.2009-1.04.

3 **Bokor Zs**, *Geopotenciális modell meghatározása CHAMP mérési adatokból a Newton-féle mozgásegyenletek felhasználásával*, Budapest University of Technology and Economics, H-1111 Műegyetem rkp 3, Budapest, Hungary, 2008. MSc Thesis.

4 **Csepregi Sz**, *Kiegyenlítő számítások*, Department of Geodesy, Faculty of Geoinformatics, University of West Hungary, 1989. Lecture Notes.

5 **Featherstone W E**, *Improvement to long-wavelength Australian gravity anomalies expected from the CHAMP, GRACE and GOCE dedicated satellite gravimetry missions*, Exploration Geophysics **34** (2003), 69–76.

6 **Földváry L**, *Determination of Satellite Velocity and Acceleration from Kinematic LEO Orbits*, Acta Geodaetica et Geophysica Hungarica **42** (2007), no. 4, 399–419, DOI 10.1556/AGeod.42.2007.4.3.

7 **Földváry L, Svehla D, Gerlach Ch, Wermuth M, Gruber Th, Rummel R, Rothacher M, Frommknecht B, Peters Th, Steigenberger P**, *Gravity model TUM-2sp based on the energy balance approach and kinematic CHAMP orbits*, Earth Observation with CHAMP - Results from Three Years in Orbit (Reigber Ch, Luhr H, Schwintzer P, eds.), Springer-Verlag, Berlin, 2004, pp. 13–18.

8 **Földváry L, Wermuth M**, *Gravity inversion techniques for High-Low SST applied to a simulated GOCE orbit*, Acta Geodaetica et Geophysica Hungarica **40** (2005), no. 1, 1–13, DOI 10.1556/AGeod.40.2005.1.1.

9 **Garcia R V**, *Local geoid determination from GRACE mission*, Ohio State University, Columbus, 2002. report 43210–1275.

10 **Lemoine F G, Kenyon S C, Factor J K, Trimmer R G, Pavlis N K, Chinn D S, Cox C M, Klosko S M, Luthcke S B, Torrence M H, Wang Y M, Williamson R G, Pavlis E C, Rapp R H, Olson T R**, *The Development of the Joint NASA GSFC and the National Imagery and Mapping Agency (NIMA) Geopotential Model EGM96*, NASA Goddard Space Flight Center, Greenbelt, Maryland, 20771 USA, July 1998. NASA/TP-1998-206861.

11 **McCarthy D D (ed.)**, *IERS Conventions*, U.S. Naval Observatory, 1996. IERS Technical Note, Vol. 21.

12 **Paizs Z, Földváry L**, *Gravitációs modell meghatározása 4 hónap GRACE mérési adatból*, Geodézia és Kartográfia **59** (2006), no. 9, 7–11.

13 _____, *Geopotenciális modell számítása GRACE mikrohullámú távolságmérés alapján*, GEOMATIKAI KÖZLEMÉNYEK **X** (2007), 201–210.

14 **Reigber Ch, Balmino G, Schwintzer P, Biancale R, Bode A, Lemoine**

J-M, Koenig R, Loyer S, Neumayer H, Marty J-C, Barthelmes F, Perosanz F, Zhu S Y, *A high quality global gravity field model from CHAMP GPS tracking data and Accelerometry (EIGEN-1S)*, Geophysical Research Letters **29** (2002), no. 14, DOI 10.1029/2002GL015064.

15 **Reigber Ch, Schwintzer P, Neumayer H, Barthelmes F, König R, Förste Ch, Balmino G, Biancale R, Lemoine J-M, Loyer S, Bruinsma S, Perosanz F, Fayard T**, *The CHAMP-only Earth Gravity Field Model EIGEN-2*, Advances in Space Research **31** (2003), no. 8, 1883–1888, DOI 10.1016/S0273–1177(03)00162-5.

16 **Reigber Ch, Schmidt R, Flechtner R, König R, Meyer U, Neumayer K-H, Schwintzer P, Zhu S Z**, *An Earth gravity field model complete to degree and order 150 from GRACE: EIGEN-GRACE02S*, Journal of Geodynamics **39** (2005), no. 1, 1–10, DOI 10.1016/j.jog.2004.07.001.

17 **Reubelt T, Austen G, Grafarend E W**, *Harmonic analysis of the Earth's gravitational field by means of semi-continuous ephemerides of a low Earth orbiting GPS-tracked satellite. Case study: CHAMP*, Journal of Geodesy **77** (2003), 257–278, DOI 10.1007/s00190-003-0322-9.

18 **Rummel R**, *Physical Geodesy*, Institut für Astronomische und Physikalische Geodäsie, Technische Universität München, 2000. Lecture Notes.

19 **Rummel R, Balmino G, Johannessen J, Visser P, Woodworth P**, *Dedicated gravity field missions - principles and aims*, Journal of Geodynamics **33** (2002), 3–20, DOI 10.1016/S0264-3707(01)00050-3.

20 **Schmidt M, Fengler M, Mayer-Gürr T, Eicker A, Kusche J, Sanchez L, Han S-C**, *Regional gravity modelling in terms of spherical base functions*, Journal of Geodesy **81** (2006), 17–38, DOI 10.1007s00190-006-0101-5.

21 **Schwarz K P**, *Fundamentals of Geodesy*, University of Calgary, 1996. ENGO 421.

22 **Timár G, Kis K, Kenyeres A**, *Short-wavelength component of the geoid: a possible indicator of the isostatic character*, 2005. Abstract No.: 7: 02636.

23 **Wermuth M, Rummel R, Földváry L**, *Mission Simulation and Semi-Analytical Gravity Field Analysis for GOCE SGG and SST*, 2006.

24 **Zaletnyik P, Völgyesi L, Paláncz B**, *Modelling local GPS/levelling geoid undulations using Support Vector Machines*, Per. Pol. Civil Eng. **52** (2008), no. 1, 39–43, DOI 10.3311/pp.ci.2008-1.06.